Phonon Thermal Transport at Interfaces of Graphene/Quasi-Hexagonal Phase Fullerene Heterostructure

Rui-Peng Wang(王瑞鹏)[1†], Tao-Tao Yu(喻涛涛)[2†], Muhammad Asif Shakoori[1], Ming-Jun Han(韩明君)[2], Yu-Xiao Hu(胡宇霄)[1], Ho-Kin Tang(邓皓键)[2*], and Hai-Peng Li(李海鹏)[1*]

[1]*School of Materials Science and Physics, China University of Mining and Technology, Xuzhou 221116, China*
[2]*School of Science, Harbin Institute of Technology, Shenzhen 518055, China*

(Received 6 January 2025; accepted manuscript online 13 March 2025)

In this study, we employed molecular dynamics simulations to investigate the interfacial thermal conductance (ITC) and phonon transport of heterostructures composed of graphene (GE) and quasi-hexagonal phase fullerene ($qHPC_{60}$). We examined the effects of size, interface interaction coefficients, and thermal equilibrium time on the ITC of the GE/$qHPC_{60}$ heterostructure. The simulation results of ITC between GE and $qHPC_{60}$ under different interlayer interaction coefficients show that an increase in interlayer interaction strength leads to a significant increase in the ITC of the heterostructure. Also, the time required for the two components to reach thermal equilibrium decreases as the interlayer interaction coefficient increases. This is attributed to the increased van der Waals forces between them, which enhance the heat transfer capability. Finally, we explored the ITC differences between the GE/$qHPC_{60}$/GE sandwich structure and the GE/$qHPC_{60}$, GE/GE, and $qHPC_{60}$/$qHPC_{60}$ bilayer structures. The interlayer interaction strength between GE and $qHPC_{60}$ layers is significantly weaker than that between the GE bilayer, leading to a reduction in ITC of GE/$qHPC_{60}$ heterostructure compared to the GE bilayer. However, higher ITC is found in the $qHPC_{60}$/$qHPC_{60}$ bilayer due to the AB stacking pattern with large interlayer interaction. This study provides insights into the potential applications of $qHPC_{60}$ based layer structures in thermal interface materials fields.

DOI: 10.1088/0256-307X/42/4/046601 CSTR: 32039.14.0256-307X.42.4.046601

1. Introduction. Thermal management is a critical factor for the performance and life of advanced materials in various applications, such as electronics, energy harvesting, and optoelectronics. With the passage of time and the struggle of researchers, devices become smaller, more powerful, and capable of operating at higher intensities, and effective heat dissipation becomes increasingly challenging. The consequence of poor thermal management is overheating, reduced efficiency, and failure of components. For improved thermal management, we need to control the thermal transport at interfaces because these interfaces show exceptional thermal behavior. The accurate knowledge and manipulation of phonon transport at these interfaces are a key approach to manage thermal transport better and overcome issues related to it. To address and contribute to these issues, heterostructure materials with suitable thermal properties will be able to overcome these issues through engineering materials interfaces. It will be possible to optimize thermal transport and enhance the efficiency of thermoelectric devices and systems. Therefore, modifying interfacial thermal resistance (ITR) has emerged as a pivotal strategy for enhancing the performance of electronic products.[1]

Carbon-based materials, including graphene, fullerenes, and others, have infused new vigor into the fabrication of electronic devices owing to their remarkable electronic structure and thermal transport capabilities. Graphene (GE), an emerging two-dimensional (2D) material, particularly distinguishes itself with its exceptionally high thermal conductivity and superb electronic properties. Experimental measurements have demonstrated that the thermal conductivity of pristine monolayer graphene is in the range between 4100–5300 W/(m·K),[2,3] indicating promising prospects in thermal interface materials for electronic devices.[4] The C_{60} molecule is a carbon sphere with a soccer ball-like shape, where each corner has an atom. The carbon sphere is composed of carbon atoms in hexagons and pentagons, such that each atom forms bonds with its three nearest neighboring atoms in sp^2 hybridization,[5] exhibits a relatively low thermal conductivity of only $\sim$0.4 W/(m·K) in bulk C_{60} (FCC).[6] Recently, Hou *et al.*[7] successfully synthesized a semiconductor quasi-hexagonal phase fullerene ($qHPC_{60}$), a new 2D carbon material with a bandgap of approximately 1.6 eV. Research has shown that $qHPC_{60}$ possesses excellent anisotropic optical,[8] mechanical,[9,10] electronic,[11–14] and thermoelectric[15] properties. The thermodynamic stability, elasticity, and fracture behavior of $qHPC_{60}$ have also been studied,[16–18] indicating that $qHPC_{60}$ is a new research platform for 2D electronics.

†These authors contributed equally to this work.
*Corresponding author. Email: denghaojian@hit.edu.cn; haipli@cumt.edu.cn
© 2025 Chinese Physical Society and IOP Publishing Ltd. All rights, including for text and data mining, AI training, and similar technologies, are reserved.

The fabrication of van der Waals (vdW) heterostructures is rapidly advancing, offering new opportunities to combine the exceptional properties of different 2D materials. The thermal conductivity of heterostructures can be significantly tuned by varying their stacking configurations, with the interface thermal behavior playing a crucial role in determining their overall performance. For instance, the in-plane thermal conductivity of GE/C_{60} heterostructure can reach about 234 W/(m·K) at room temperature, which exceeds that of many pure metals. In addition, the in-plane and interfacial heat transfer characteristics can be influenced by adjusting the interfacial interaction coefficient.[19] When a single layer of GE is overlaid on phosphorene, the resulting mixed vdW bilayer becomes a potential candidate for high-performance thermal/electronic applications, leveraging the direct bandgap properties of phosphorene combined with the ultrahigh thermal conductivity of GE.[20] Due to interlayer vdW interactions, in-plane heat transfer is often inhibited. Relative to single-layer qHPC$_{60}$, low-frequency phonon modes in bilayer qHPC$_{60}$ exhibit a redshift, leading to a decrease in the group velocity and mean free path of low-frequency phonons, and, consequently, a reduction in thermal conductivity.[21] For Silicene/GE heterostructures, the GE layer serves as the primary thermal transport pathway in the heterostructure and thus, the introduction of a GE substrate can significantly enhance the thermal dissipation of Silicene/GE heterostructure devices.[22] Recently, Yu *et al.*[23] explored the mechanical properties of the GE/qHPC$_{60}$ heterostructure through heterogeneous stacking and found that using GE sheets as substrates or encapsulation can effectively enhance the tensile strength and mechanical stability of 2D fullerene, showing promising application in flexible electronics. However, there have been few studies on thermal transport in GE/qHPC$_{60}$ heterostructures. Here we employed molecular dynamics simulations to study the interfacial thermal conductance of GE/qHPC$_{60}$ heterostructures and further explained the impact of increased interlayer interactions on interlayer heat transfer through phonon heat transfer characteristics. The conclusions of this study provide valuable insights into the thermal transport properties of GE/qHPC$_{60}$ heterostructures as well as more extensive van der Waals (vdW) heterostructures.

2. Method and Model. Figure 1 displays a schematic diagram of the GE/qHPC$_{60}$ heterostructure, with graphene forming the upper layer and a 2D quasi-hexagonal fullerene comprising the lower layer. The AIREBO potential[24,25] was applied to describe the C-C interactions in the GE and qHPC$_{60}$ monolayers, and this potential has been widely used to calculate the thermal conductivity of graphene-based nanomaterials.[26,27] The inter-layer interaction between GE and qHPC$_{60}$ heterostructure is expressed by Lennard-Jones (LJ) potential,

$$V(r_{ij}) = 4\varepsilon\chi\left[\left(\frac{\sigma}{r_{ij}}\right)^{12} - \left(\frac{\sigma}{r_{ij}}\right)^{6}\right], \tag{1}$$

where ε is the depth of potential well, σ is the distance

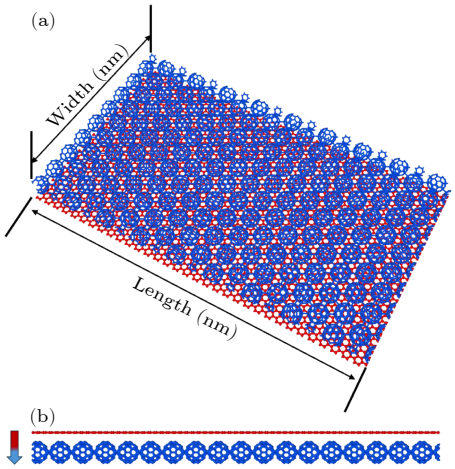

Fig. 1. Schematic diagram of GE/qHPC$_{60}$ heterostructure, (a) vertical viewand (b) side view.

at which the interparticle potential is zero, and r_{ij} is the distance between carbon atom i and j. χ is a scaling factor used to adjust the strength of the interaction. Here, the parameters of LJ potential are $\varepsilon = 2.688$ meV and $\sigma = 4.01$ Å.

The molecular dynamics (MD) simulations were conducted using the LAMMPS software.[28] The simulation time step was set to 0.5 fs, with the periodic boundary conditions applied in the x and y directions. In the relaxation process of the heterostructure system followed these three steps: first, a 250 ps relaxation in the NVT ensemble at 300 K, then increased the temperature to 500 K for another 250 ps relaxation. The system was then cooled back to 300 K for a final 250 ps relaxation. This process was repeated twice, followed by a 500 ps relaxation was performed in the NVE ensemble to ensure the system reached thermodynamic equilibrium. To calculate interface thermal resistance (ITR), the heat dissipation method[29,30] was implemented in the fully relaxed system. The ITR calculation procedure involved rapidly heating the upper GE layer to 500 K during 250 fs, while the temperature of the lower qHPC$_{60}$ layer is kept at 300 K. Here, a thermal exchange algorithm is employed to adjust the rate of energy transport continuously,[31] facilitating the rapid rise in temperature of the GE layer. After 250 fs, the thermostat is turned off, allowing heat to transfer from the upper GE layer to the lower qHPC$_{60}$ layer. After 500 ps, the GE and qHPC$_{60}$ layers reach a new equilibrium state, as shown in Fig. 2(a). The temporal variations in energy dissipation of the upper GE over time is described as follows:

$$\frac{\partial E_t}{\partial t} = \frac{A}{R}(T_{\mathrm{GE}} - T_{\mathrm{qHPC_{60}}}), \tag{2}$$

where R is the ITR, A is the area of the heterostructure interface, $T_{\mathrm{GE}} - T_{\mathrm{qHPC_{60}}}$ is the temperature difference between GE and qHPC$_{60}$ layers, and E_t is the energy of the GE layer.

The energy E_t after integration becomes as

$$E_t = E_0 + \frac{A}{R}\int_0^t (T_{\mathrm{GE}} - T_{\mathrm{qHPC_{60}}})\mathrm{d}t, \tag{3}$$

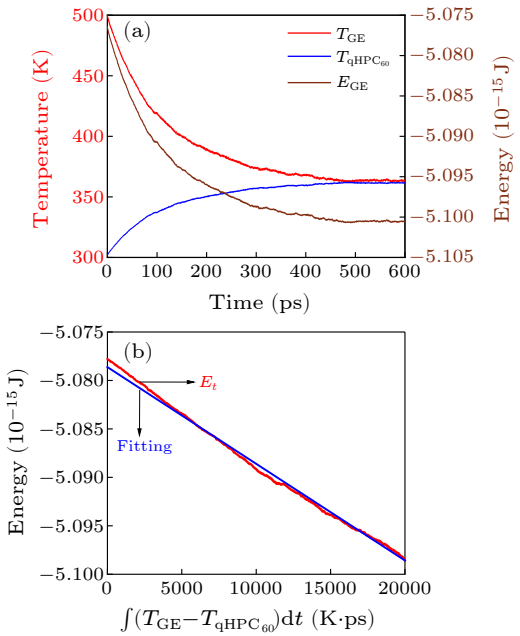

Fig. 2. (a) The evolution of the GE temperature (T_{GE}), qHPC$_{60}$ temperature ($T_{qHPC_{60}}$), and energy of the GE energy (E_{GE}) on time t during the heat dissipation process; (b) The linear relationship between E_{GE} and time-integrated temperature difference ($T_{GE} - T_{qHPC_{60}}$) during the heat transfer, assuming the flow of heat from GE layer to the qHPC$_{60}$ layer.

where E_0 is the initial energy dissipated by GE heat, as shown in Fig. 2(b), and the ITR (R) is obtained by linear fitting. In order to verify the reliability and accuracy of the used method, we selected a GE/qHPC$_{60}$ vdW heterostructure with an interface area of 14.2 nm×8.2 nm, and the distance between the layers is 0.34 nm. The calculated interfacial thermal conductance(ITC) of the GE/qHPC$_{60}$ heterostructure is $G = 1/R = \sim 8.7\,\mathrm{MW/(K{\cdot}m^2)}$. In the present paper, for each set of ITC data, we performed six independent simulations to suppress the errors.

Phonon density of state (PDOS) is an important parameter that reflects the thermal properties of crystals at the microscopic level. The degree of overlap in the PDOS between layered materials determines the phonon transmission behavior of the interface. Experimentally, the PDOS can be measured by using inelastic neutron scattering techniques. Through MD simulations, PDOS can be derived from the Fourier transform of the velocity autocorrelation function as described by [32,33]

$$D(\omega) = \int_0^{\tau} \Gamma(t) \exp(-\mathrm{i}\omega t)\mathrm{d}t, \tag{4}$$

where ω is the frequency, $D(\omega)$ is the PDOS as a function of frequency, $\Gamma(t)$ is the velocity autocorrelation function, defined as $\Gamma(t) = \langle \nu(t) \cdot \nu(0) \rangle$. The ITR between heterostructure interfaces is closely related to the PDOS overlap factor S of the materials on both sides of the interface,

$$S = \frac{\int_0^{+\infty} D_1(\omega) D_2(\omega)\mathrm{d}\omega}{\int_0^{+\infty} D_1(\omega)\mathrm{d}\omega \int_0^{+\infty} D_2(\omega)\mathrm{d}\omega}, \tag{5}$$

where D_1 and D_2 are the PDOS of the materials on both sides of the interface. The values of the overlap factor S are directly related to the phonon coupling strength between the two layers.

3. Results and Discussion. The effects of varying widths and lengths on the ITC of the GE/qHPC$_{60}$ heterostructure were systematically analyzed in a sequence to elucidate their roles in heat transfer. Temperature variations of the GE and qHPC$_{60}$ layers over simulation time are shown in Fig. 2(a). Notably, after 500 ps, the temperature of the GE layer decreases from 500 K to around 360 K, rather than the intermediate value of 400 K. This discrepancy is due to the higher thermal conductivity of the GE layer compared to qHPC$_{60}$, which results in more efficient dissipation. First, we fixed the length at 14.2 nm and varied the width across four values: 2.7, 5.5, 8.2, and 10.9 nm. The effects of width on the ITC are demonstrated in Fig. 3(a), where heat is transferred from the GE layer to the qHPC$_{60}$ layer. It is found that with increasing the width from 2.7 nm to 10.9 nm, the ITC between GE and qHPC$_{60}$ converges to approximately 8.7 MW/(K·m^2), suggesting that beyond a certain width, the impact of width on the ITC becomes negligible. Next, we analyze the effects of varying lengths of both layers on ITC, which are calculated by keeping the width constant at 8.2 nm, see Fig. 3(b). Four different lengths (= 4.7, 9.5, 14.2, and 18.9 nm) are chosen for this analysis as shown in Fig. 3(b), aiming to explore their respective impacts comprehensively. The simulation results reveal that as the lengths of both layers increase, the ITC between GE and qHPC$_{60}$ remains largely unchanged, stabilizing at about 8.7 MW/(K·m^2). This indicates that within a certain size range, the impact of the dimensions of the GE/qHPC$_{60}$ heterostructure does not significantly influence ITC. This behavior is consistent with similar earlier studies on GE/black phosphorus heterostructure interface, where ITC was also found to be relatively insensitive to changes in length and width within certain ranges. [24] Considering the minimal effect of length and width on ITC within the studied ranges and considering computational efficiency, we selected a width of 8.2 nm and a length of 14.2 nm for further studies on the influence of interlayer interactions on the ITC of the GE/qHPC$_{60}$ heterostructure.

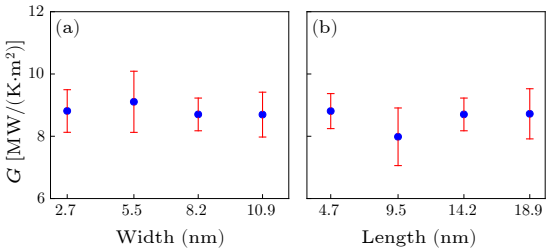

Fig. 3. Interfacial thermal conductance (G) versus (a) width and (b) length for GE/qHPC$_{60}$ heterostructure.

After a comprehensive analysis of the effects of width and length on ITC, we next investigate the effects of varying χ between the GE and qHPC$_{60}$ layers. The χ is a key parameter that measures the strength of energy coupling between the two materials at their interface,

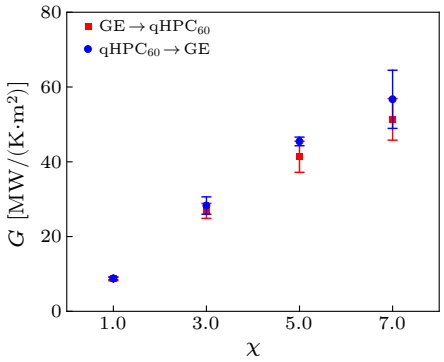

Fig. 4. Interfacial thermal conductance (G) of GE/qHPC$_{60}$ heterostructure with different interface interaction coefficients χ from 1.0 to 7.0.

influencing the efficiency of heat transfer. As we know, the heterostructure experiences vdW forces between GE and qHPC$_{60}$ layers. For this, LJ potential [Eq. (1)] is used to tune the interlayer interaction strength by changing χ. In our simulations, we varied the interface interaction coefficient from 1.0 to 7.0, and the results reveal a clear trend: as the interaction coefficient increases, the ITC increases significantly, with the ITC from GE to qHPC$_{60}$ rising from 8.7 MW/(K·m^2) at a coefficient of 1.0 to 51.3 MW/(K·m^2) at a coefficient of 7.0. Similarly, the ITC in the reverse direction (from qHPC$_{60}$ to GE) increases from 8.78 MW/(K·m^2) at a coefficient of 1.0 to 56.7 MW/(K·m^2) at a coefficient of 7.0. These trends, illustrated in Fig. 4, highlight the critical role of the χ in governing heat transfer at the heterostructure interface. A higher χ enhances interlayer interactions, allowing phonons to move more easily from the high-temperature layer to the low-temperature layer, making the phonon heat transfer between the GE and qHPC$_{60}$ layers more efficient, thereby increasing the overall ITC. We found that the value of χ significantly affects the ITC between GE and qHPC$_{60}$, as revealed in the earlier work.[19] Moreover, these results are consistent with previous studies on other 2D heterostructures, such as the phosphorene/h-BN[34] and GE/MoS$_2$[35] interfaces, where similar trends of increasing ITC with stronger interface coupling have been observed, albeit with some variation in the saturation behavior. Overall, these results demonstrate the substantial impact of the interface interaction coefficient on the thermal behavior of the GE/qHPC$_{60}$ heterostructure. It suggests that by carefully tuning the χ, it is possible to significantly enhance the thermal performance of the system, which is of great importance for the design of efficient thermal management solutions in applications such as microelectronics, thermoelectrics, and heat dissipation in nanoscale devices.

In addition to examining the ITC, we further investigate the out-of-plane PDOS and overlap factor (S) between GE and qHPC$_{60}$ layers, as these factors are essential for understanding phonon thermal transport at the interface. The out-of-plane PDOS modes, in particular, are very important for heat transfer in heterostructures.

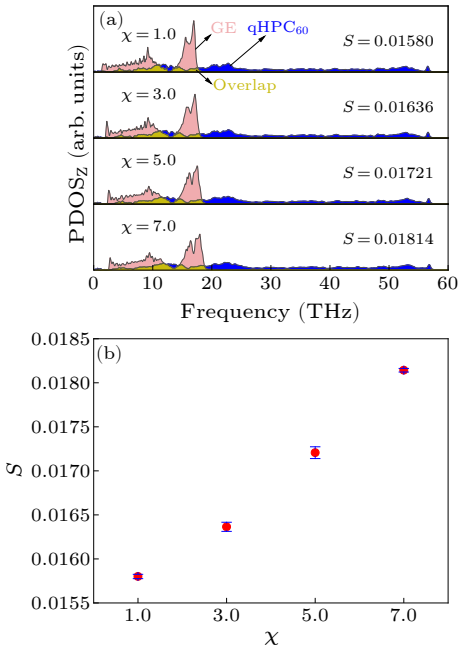

Fig. 5. (a) The out-of-plane PDOS (PDOS$_Z$) and (b) PDOS$_Z$ overlap factor S for the interfacial interaction coefficient χ ranging from 1.0 to 7.0 in the GE/qHPC$_{60}$ heterostructure.

As shown in Fig. 5(a), the out-of-plane PDOS of GE and qHPC$_{60}$ exhibits a significant overlap within the vibrational frequency range of 0–20 THz. This overlap is similar to what has been observed in the GE-based heterostructures, such as the GE/C$_{60}$ heterostructure.[19] With increasing χ, the interlayer interactions between the GE and qHPC$_{60}$ are enhanced. This enhanced interaction leads to atomic vibrations in one layer being more effectively scattered by atoms in the other layer causing atomic vibrations in one layer to be strongly scattered by atoms in another layer. As shown in Fig. 5(b), the increase in χ indirectly enhances the anharmonicity of the system and strengthens the phonon coupling between the graphene and qHPC$_{60}$ layers. Consequently, the overlap factor increases with the increase in χ, further enhancing the interlayer phonon heat transfer capability at the interface, promoting effective heat transfer between the two materials. This can explain the observed increase in ITC as χ increases. This behavior is consistent with previous studies on other heterostructure, such as GE/C$_3$N[36] and GE/MoSe$_2$.[37] In summary, our findings emphasize the crucial role of phonon coupling in interfacial heat transfer in the GE/qHPC$_{60}$ heterostructure.

Moreover, as shown in Fig. 6, the effect of increasing χ is clearly evident in the faster thermal equilibration between the GE and qHPC$_{60}$ layers. With the increase in χ, we observe a significant reduction in the time required for GE/qHPC$_{60}$ to reach thermal equilibrium. For instance, when χ is 3.0, the time needed for thermal equilibrium is approximately one-third of that when χ is 1.0. This rapid equilibration at higher χ values further underscores the role of interlayer interactions in enhancing phonon coupling, which accelerates heat transfer across the interface.

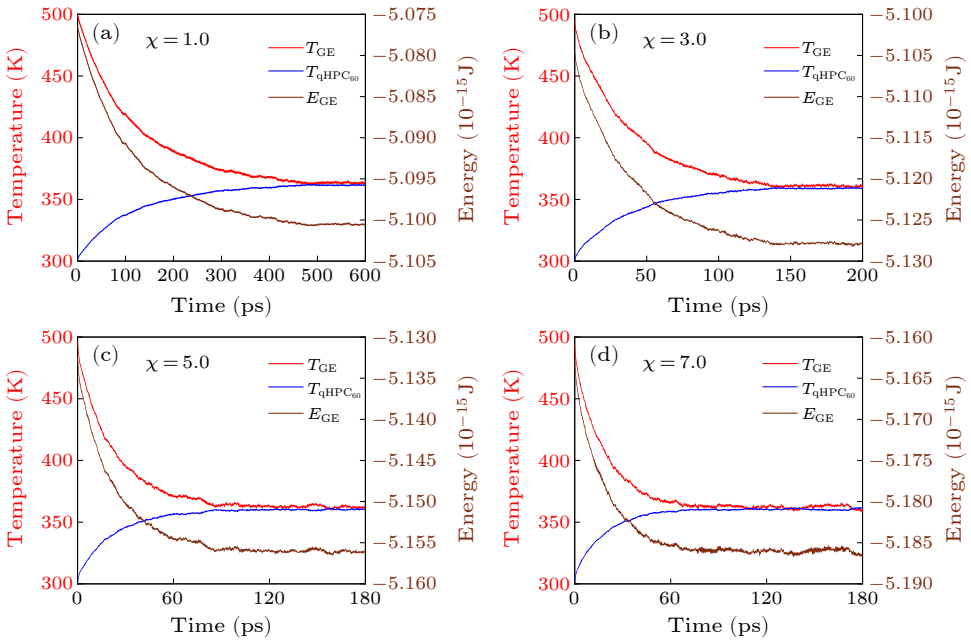

Fig. 6. Variations in the temperature of GE/qHPC$_{60}$ and the GE energy under different interface interaction coefficients (a)–(d): $\chi = 1.0,\ 3.0,\ 5.0,\ 7.0$.

As the interface interaction strength increases, the phonon transmission becomes more efficient, leading to quicker temperature stabilization between the two materials. This behavior highlights the importance of interface engineering, where optimizing χ can be a powerful tool for improving heat dissipation efficiency, crucial for applications in thermoelectric devices, microelectronics, and other nanoscale systems.

Finally, we investigated the ITC of the GE/qHPC$_{60}$/GE sandwich structure and compared its ITC with those of bilayer structures (including GE/GE, qHPC$_{60}$/qHPC$_{60}$, GE/qHPC$_{60}$), as detailed in Table 1. Both GE/qHPC$_{60}$/GE sandwich structure and GE/qHPC$_{60}$ bilayer exhibit significantly lower ITC than the GE/GE structure does. This difference can be comprehensively understood from the perspective of phonon transport at the interface. Phonons, as quantized energy units representing lattice vibrations, are intrinsically linked to heat conduction. In the bilayer GE/GE system, the interface between the identical GE layers is relatively smooth. This enables phonons to traverse seamlessly from one GE layer to the other, maintaining favorable propagation characteristics. As a result, the thermal transport performance is relatively excellent, as evidenced by a relatively high ITC. In contrast, within the GE/qHPC$_{60}$ heterostructure, the spherical geometry of qHPC$_{60}$ gives rise to point-to-surface contact with GE. This not only decreases the contact area and weakens the interaction between the two materials but also typically leads to a larger interface roughness compared to the GE/GE interface. Consequently, the enhanced interface roughness induces more intense scattering of phonons at the GE/qHPC$_{60}$ interface, significantly diminishing the ITC. Regarding the GE/qHPC$_{60}$/GE sandwich structure, it features two GE/qHPC$_{60}$ interfaces. During phonon propagation, they encounter scattering at these two interfaces successively. This double-scattering event further impedes the overall thermal transport efficiency, thereby resulting in an even lower ITC. Additionally, when the direction of heat transfer is reversed, the ITC of the GE/qHPC$_{60}$ heterostructure also slightly alters, as shown in Table 1. This difference in ITC becomes more pronounced as χ it increases, as illustrated in Fig. 4, further supporting the presence of thermal rectification.[38] It should be noted that the qHPC$_{60}$/qHPC$_{60}$ bilayer with 12.8 nm × 9.1 nm interface exhibits an AB stacking pattern, where the fullerene spheres are densely packed between layers. This close interface contact results in strong vdW interactions in qHPC$_{60}$/qHPC$_{60}$. This configuration facilitates more effective interlayer heat transfer in qHPC$_{60}$/qHPC$_{60}$, showcasing a relatively higher ITC compared to other bilayer structures studied.

Table 1. ITC of GE/GE, qHPC$_{60}$/qHPC$_{60}$, GE/qHPC$_{60}$ and GE/qHPC$_{60}$/GE.

Model	G [MW/(K·m^2)]
GE/GE	22.67 ± 1.37, ∼36[39], ∼33[40]
qHPC$_{60}$/qHPC$_{60}$	30.89 ± 1.94
GE(hot)/qHPC$_{60}$ (cold)	8.70 ± 0.52
GE(cold)/qHPC$_{60}$ (hot)	8.78 ± 0.33
GE(hot)/qHPC$_{60}$/GE(cold)	7.90 ± 0.43

4. Conclusion. In summary, we employed molecular dynamics simulations to investigate the ITC and phonon transport of GE/qHPC$_{60}$ heterostructures. It was found that within a certain size range, the size of the GE/qHPC$_{60}$ heterostructure has minimal impact on the ITC, demonstrating size-insensitive behavior. Additionally, we examined the strong correlation between the ITC and the interlayer interaction coefficient (or interlayer interaction strength) in the GE/qHPC$_{60}$ heterostruc-

ture. As the interlayer interaction coefficient increased, the ITC was significantly enhanced, revealing a positive correlation and uncovering the thermal rectification effect in the GE/qHPC$_{60}$ heterostructure. Furthermore, we found that as the interlayer interaction coefficient between GE and qHPC$_{60}$ increased, the enhanced interlayer interactions accelerated the achievement of thermal equilibrium. Finally, we carry out comparative analysis of the ITC of the GE/qHPC$_{60}$/GE, GE/qHPC$_{60}$, GE/GE and qHPC$_{60}$/qHPC$_{60}$. The interlayer interaction strength between GE and qHPC$_{60}$ layers is significantly weaker than that between GE bilayer, leading to a reduction in ITC of GE/qHPC$_{60}$ heterostructure compared to GE bilayer. However, we found most higher ITC in qHPC$_{60}$/qHPC$_{60}$ bilayer due to the AB stacking pattern, showing promising application in thermal interface materials.

Acknowledgements. This work was supported by the National Natural Science Foundation of China (Grant No. 12204130), the Fundamental Research Funds for the Central University of China (Grant No. 2019ZDPY16) and the Basic Research Project of Xuzhou City (Grant No. KC22043). Ruipeng Wang and Yuxiao Hu acknowledge the support funded by the Graduate Innovation Program of China University of Mining and Technology (Grant Nos. 2024WLJCRCZL266 and 2024WLJCRCZL294) and the Postgraduate Research Practice Innovation Program of Jiangsu Province (Grant No. KYCX24_2692).

References

[1] Li M, Shakoori M A, Wang R, and Li H 2024 *Chin. Phys. Lett.* **41** 016302
[2] Wei Y, Li K, and Tang K 2019 *Accid. Anal. Prev.* **123** 324
[3] Ghosh S, Calizo I, Teweldebrhan D, Pokatilov E, Nika D, Balandin A, Bao W, Miao F, and Lau C 2008 *Appl. Phys. Lett.* **92** 151911
[4] Song H and Kang F 2022 *Acta Phys. -Chim. Sin.* **38** 202101013
[5] David W I F, Ibberson R M, Matthewman J C, Prassides K, Dennis T J S, Hare J P, Kroto H W, Taylor R, and Walton D R M 1991 *Nature* **353** 147
[6] Tea N H, Yu R C, Salamon M B, Lorents D C, Malhotra R, and Ruoff R S 1993 *Appl. Phys. A* **56** 219
[7] Hou L, Cui X, Guan B, Wang S, Li R, Liu Y, Zhu D, and Zheng J 2022 *Nature* **606** 507
[8] Yu L, Xu J, Peng B, Qin G, and Su G 2022 *J. Phys. Chem. Lett.* **13** 11622
[9] Mortazavi B and Zhuang X 2022 *Coatings* **12** 1171
[10] Giannopoulos G I, Georgantzinos S K, and Ghavanloo E 2024 *Adv. Theory Simul.* **7** 2400566
[11] Argaman U and Makov G 2023 *npj Comput. Mater.* **9** 211
[12] Chernozatonskii L A and Kochaev A I 2024 *Polymers* **16** 1580
[13] Yadav S, Sadhukhan S, and Yadav V K 2024 *Appl. Surf. Sci.* **676** 161003
[14] Wang R, Li H, Shakoori M A, Cheng X, Hu Y, and Wang L 2024 *J. Appl. Phys.* **136** 015101
[15] Peng B 2023 *Nano Lett.* **23** 652
[16] Ying P, Dong H, Liang T, Fan Z, Zhong Z, and Zhang J 2023 *Extreme Mech. Lett.* **58** 101929
[17] Shen G, Li L, Tang S, Jin J, Chen X J, and Peng Q 2023 *Crystals* **13** 224
[18] Ribeiro L A, Pereira M L, Giozza W F, Tromer R M, and Galvão D S 2022 *Chem. Phys. Lett.* **807** 140075
[19] Ma H, Babaei H, and Tian Z 2019 *Carbon* **148** 196
[20] Hong Y, Zhang J, and Zeng X C 2016 *Nanoscale* **8** 19211
[21] Yang C, Wang A, Qi H, Wang W, Ji W, and Wang X 2024 *Int. J. Heat Mass Transfer* **222** 125197
[22] Zhou J, Li H, Tang H K, Shao L, Han K, and Shen X 2022 *ACS Omega* **7** 5844
[23] Yu T, Li J, Han M, Zhang Y, Li H, Peng Q, and Tang H K 2023 *Nanomater.* **13** 1936
[24] Chen Y, Zhang Y, Cai K, Jiang J, Zheng J C, Zhao J, and Wei N 2017 *Carbon* **117** 399
[25] Stuart S J, Tutein A B, and Harrison J A 2000 *J. Chem. Phys.* **112** 6472
[26] Fox A, Ray U, and Li T 2019 *J. Appl. Phys.* **125** 015101
[27] Wang C, Lu S, Yu X, and Li H 2019 *Chin. Phys. B* **28** 016501
[28] Plimpton S 1995 *J. Comput. Phys.* **117** 1
[29] Zhang J, Wang Y, and Wang X 2013 *Nanoscale* **5** 11598
[30] Wu B, Zhou M, Xu D, Liu J, Tang R, and Zhang P 2022 *Surf. Interf.* **32** 102119
[31] Ikeshoji T and Hafskjold B 1994 *Mol. Phys.* **81** 251
[32] Liu B, Reddy C D, Jiang J, Baimova J A, Dmitriev S V, Nazarov A A, and Zhou K 2012 *Appl. Phys. Lett.* **101** 211909
[33] Mollow B R 1969 *Phys. Rev.* **188** 1969
[34] Li T 2021 *Physica E* **131** 114761
[35] Liu B, Meng F, Reddy C D, Baimova J A, Srikanth N, Dmitriev S V, and Zhou K 2015 *RSC Adv.* **5** 29193
[36] Han D, Wang X, Ding W, Chen Y, Zhang J, Xin G, and Cheng L 2018 *Nanotechnology* **30** 075403
[37] Hong Y, Ju M G, Zhang J, and Zeng X C 2018 *Phys. Chem. Chem. Phys.* **20** 2637
[38] Zhao J N, Liu D H, Wei D, and Shang X C 2020 *Acta Phys. Sin.* **69** 056501
[39] Yang Z Q, Shakoori M A, and Li H P 2024 *AAPPS Bull.* **34** 1
[40] Xue Y, Park H S, and Jiang J W 2023 *Int. J. Heat Mass Transfer* **212** 124222